



# Dynamic Response of Pillar Workings Induced by Sudden Pillar Recovery

Zilong Zhou<sup>1</sup> · Yuan Zhao<sup>1</sup> · Wenzhuo Cao<sup>2</sup> · Lu Chen<sup>1</sup> · Jing Zhou<sup>1</sup>

Received: 2 October 2017 / Accepted: 13 May 2018 / Published online: 19 May 2018  
© Springer-Verlag GmbH Austria, part of Springer Nature 2018

## Abstract

When residual pillars are extracted in a short time in room and pillar mining, the load transferred from the removed pillar acts on neighbouring pillar workings in a dynamic manner. This study aims to investigate the instability of large mined-out areas triggered by dynamic disturbance resulting from residual pillar recovery. A mechanical model combining the pressure arch theory (PAT) based method and structural dynamics was first established to assess the stress state and deformation of a pillar subjected to combined effects of static and dynamic loads. The process of residual pillar recovery and potential induced instability of neighbouring pillar workings in a five-pillar system was further numerically simulated in both static and dynamic modes, and the response of adjacent pillars was investigated. It was found that the induced disturbance to a pillar can be characterised by the dynamic amplification coefficient  $R$ , the ratio of the increased vertical pillar load to the transferred load.  $R_{\max}$  can exceed 1.5 or even approach 2 in practical pillar recovery using the blasting method. Modelling results showed that while pillar workings adjacent to a removed pillar remain stable in static analysis, violent and large-scale pillar collapses can be triggered in the event of quick pillar recovery of blasting method. Results indicated that when the dynamic effect of pillar recovery is not considered, the load undertaken by adjacent pillar workings would be largely underestimated. To ensure mining safety, the induced dynamic effect should be accounted for in the design of the pillar recovery method.

**Keywords** Unloading process · Dynamic disturbance · Rock failure · Initial stress · Pillar instability

## Abbreviations

DEM	Discrete element method
PAT	Pressure arch theory
$D$	Fraction of critical damping
$E$	Elastic modulus of a pillar
EA	Excavated area
$e$	Extraction ratio
$g$	Gravitational acceleration
$H$	Depth of pillars
$K$	Elastic stiffness of a pillar
LTD	Load transfer distance
$m$	Mass of a pillar
$R$	Dynamic amplification coefficient
$r$	Pillar radius
$T$	Natural vibration period of a pillar

$t_0$	Load transfer duration
$U$	Total released energy in extraction
$U_d$	External energy from the dynamic disturbance
$U_f$	Energy needed to be consumed in fracturing rock masses
$U_s$	Strain energy stored in the rock mass to be extracted
$w_e$	Effective width for non-square pillars
$y_s$	Pillar deformation increment
ZI	Area of zone of influence
$\alpha$	Damping coefficient
$\rho$	Rock density
$\sigma_{\text{cri}}$	Critical stress
$\sigma_d$	Dynamic vertical pillar load
$\Delta\sigma_d$	Dynamic transferred vertical pillar load
$\sigma_{H_{\max}}$	The maximum horizontal principal stress
$\sigma_s$	Static (final) vertical pillar load
$\Delta\sigma_s$	Static (final) transferred vertical pillar load
$\sigma_v$	Vertical stress
$\sigma_v$	Vertical pillar load
$\sigma_v^{\max}$	The maximum vertical pillar load
$\Omega$	Natural vibration frequency of a pillar

✉ Wenzhuo Cao  
w.cao15@imperial.ac.uk

<sup>1</sup> School of Resources and Safety Engineering, Central South University, Changsha, Hunan 410083, China

<sup>2</sup> Department of Earth Science and Engineering, Royal School of Mines, Imperial College, London SW7 2AZ, UK

## 1 Introduction

A flatly dipping orebody is usually mined by the room and pillar method. A grid of rooms is extracted on a horizontal plane, leaving large mined-out areas in deep underground. According to statistical data, a total of 1.28 billion square metres of mined-out areas were left in metal and non-metal mines in China by the end of 2015. In these areas, pillar workings act as supporting structures to support huge overburden (Zhou et al. 2018b). For the sake of increasing mine life and total return on investment, parts of residual pillars are extracted after room extraction, and vertical loads are redistributed and applied on adjacent pillar workings. Under higher stress levels, it may trigger the instability of neighbouring pillar workings, or even give rise to catastrophic progressive pillar collapses in large mined-out areas.

The calculation of vertical pillar load before and after extraction and the stability evaluation of mined-out areas attract intensive research efforts (Chen et al. 2017; Xiao et al. 2017; Zhang et al. 2017). The tributary area method has been widely used for estimating average axial stress states in coal pillars (Brady and Brown 2013). The fundamental assumption of this method is that each pillar carries the full load of the overlying strata, and half of that of surrounding roadways. Abel (1988) used the parabolic load transfer arch for estimation of loads undertaken by yield and barrier pillars in soft rock. The pressure arch theory (PAT) based method proposed by Poulsen (2010) could account for both pillar geometry and the spatial position within the panel, and was successfully applied for risk assessment of a decommissioned colliery in Australia (Poulsen and Shen 2013). When pillars are of approximately regular shapes and can be treated as linearly elastic media, reliable estimation of vertical pillar stresses can be obtained in three-dimensional numerical simulation (Brady and Brown 2013). Lunder and Pakalnis (1997) proposed an estimation method for hard rock pillar strength by integrating the tributary area method and boundary element analysis, so as to reconcile empirical expressions of pillar stress with more rigorous analysis.

As pillars are usually extracted in a very short time, the transferred load would act on neighbouring pillars in a dynamic manner, introducing distinct excitation to adjacent pillars and surrounding strata. However, previous research work only accounted for the final transferred load based on the extraction ratio change after pillar recovery, and little effort went into investigation of the dynamic load transfer process and the accompanying induced disturbance. The risk assessment of mined-out areas is based on the estimation of pillar loads and load transfer after extraction, and the goaf stability can thus be

overestimated. In this regard, the dynamic pillar recovery induced disturbance and possibly triggered instability of mined-out areas should be investigated.

Actually, dynamic disturbance resulting from caving, blasting, and extraction, etc., is quite common in deep underground (Kaiser et al. 1996; Kaiser and Cai 2012; Cao et al. 2018; Li et al. 2018; Zhao et al. 2018). It was reported that underground coal pillar recovery accompanied with caving of overlying strata could cause dynamic loading over neighbouring pillars (Singh et al. 2011a, b). The dynamic disturbance can be remarkable when underground coal pillars lie under strong and massive roof strata. Previous studies also revealed that dynamic response of surrounding rock can be induced by the excavation unloading of underground openings (Lu et al. 2012; Li et al. 2014). The induced peak particle velocity (PPV) in surrounding rock increases with increasing unloading rates (Cao et al. 2016).

Excavation induced dynamic disturbance has a detrimental effect on the stability of underground openings and structures (Kaiser et al. 1996; Tao et al. 2013; Yang et al. 2013). For example, the instantaneous tunnel excavation in high initial stress states can lead to the dynamic stress concentration around adjacent tunnels, and even damage and failure on the incident side of the tunnel (Li et al. 2016). Dynamic disturbance from blast loading, like rheological loads and water, can cause deterioration in mechanical properties of rock masses, and thus reduce the stability of goaf (Chao et al. 2015; Zhou et al. 2018a). For mined-out areas left by the room and pillar method, the induced dynamic disturbance is also a significant cause to its instability. Understanding the mechanism and associated consequences of dynamic disturbance is necessary to prevent these hazards. The Canadian Rockburst Support Handbook (Kaiser et al. 1996) summarised a number of case studies of seismically induced rockbursts, and suggested that rock support in burst-prone ground needs to resist dynamic loads and large rock dilation due to violent rock failure. Wang et al. (2013) simulated the dynamic mechanical state evolution of a coal pillar during longwall mining using FLAC3D, and found that the vertical pillar stress could be used as a precursor to coal bump occurrences. Wang et al. (2016) simulated the dynamic response of a coal pillar under seismic disturbance caused by roof caving, and found the pillar width-to-height ( $W/H$ ) ratio to be an important factor influencing the response. Dynamic behaviour of pillars in response to disturbance is negligible at large  $W/H$  ratios (greater than 4), but can be quite apparent at small ones (lower than 2).

This research focuses on the dynamic disturbance resulting from pillar recovery and the induced instability of adjacent pillar workings. In Sect. 2, the dynamic response of pillar workings to pillar recovery is simplified to a problem of one-dimensional loading on a pre-stressed pillar. In Sect. 3, a mechanistic model is developed to evaluate the

stress state and deformation of pillar workings adjacent to a removed pillar, in which the maximum vertical pillar load is calculated based on the pressure arch theory and structural dynamics. In Sect. 4, numerical simulation using the discrete element code PFC2D is carried out to model the response of a five-pillar system subjected to the central pillar recovery in both static and dynamic modes. The influence of pillar recovery time on the stability of pillar workings is further discussed.

## 2 Dynamic Stress Disturbance Induced by Pillar Recovery

In inclined orebodies, some room-and-pillar type pillars are designed to be oriented perpendicular to the footwall and hanging wall, and thus are subjected to compressive and shear stresses (Suorinen et al. 2011, 2014). Far-field major principal stress inclination of  $15^\circ$  or more relative to orebodies is significant to cause weakening in pillars workings. In this work, only vertically designed pillar workings dominated by compressive stress are considered, so as to minimise the impacts of shear loading on the behaviour of pillars.

It is widely accepted that pillar workings adjacent to a removed pillar are prone to be damaged or even crushed by load transferred from the removed pillar. However, in the perspective of dynamics, the response of neighbouring pillars is caused by unloading disturbance emanating from the removed pillar. Specifically, loads acting on the top and bottom of an excavated pillar can be replaced by statically equivalent stresses. Instantaneous pillar recovery means sudden unloading of the equivalent stresses, initiating a dynamic unloading wave travelling away from the removed pillar. All rock particles subjected to this wave tend to move towards the opposite direction of wave propagation. When the wave reaches adjacent pillar workings, the exerted force acts on both the top and bottom of pillars in the loading direction. Adjacent pillar workings, therefore, are subjected to the combined effects of the initial vertical stress (Fig. 1a), and the dynamic disturbance from rock masses (Fig. 1b). The dynamic stress acting on adjacent pillars oscillates in a short time, and eventually converges to a fixed value equal to the redistributed overburden.

With a large pillar spacing, the effect of incident wave's curvature is marginal, and the wave can be roughly treated as an elastic plane wave for adjacent pillars (Pao and Mow 1973). In this respect, the dynamic response of pillar workings induced by pillar recovery can be simplified to a problem of one-dimensional loading on a pre-stressed pillar. The dynamic behaviour of adjacent pillar workings is closely related to the stress level, pillar spacing and extraction time, etc.

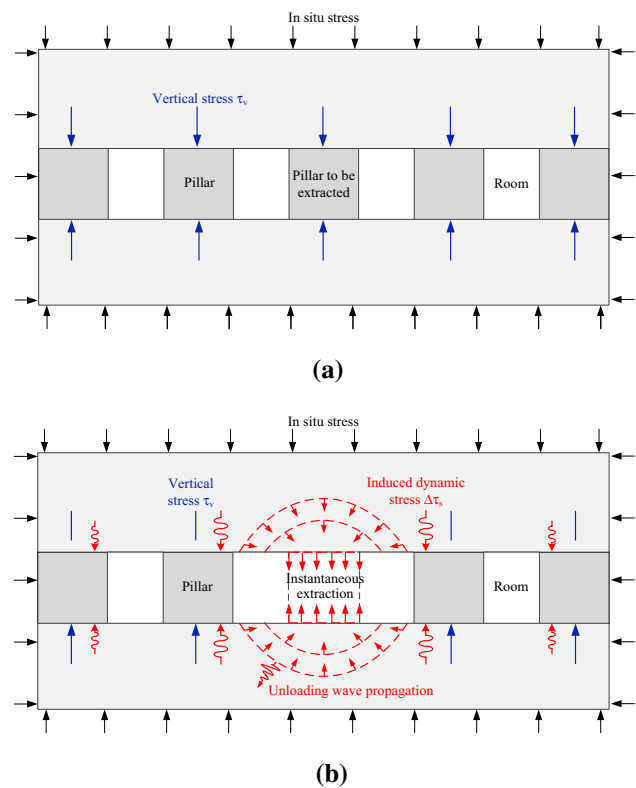


**Fig. 1** Schematic of instantaneous pillar recovery and induced dynamic response of adjacent pillar workings: **a** before pillar recovery, and **b** after pillar recovery

## 3 Induced Dynamic Stress Concentration and Instability of Pillar Workings

As introduced in Sect. 2, the induced dynamic response of vertical pillars is primarily associated with the initial vertical stress, the transferred load, and the compressive strength of pillars. In this section, the pillars are assumed to be linearly elastic before failure and of regular shape. The initial and transferred vertical pillar loads will be first calculated, on the basis of which the dynamic pillar behaviour and pillar collapse in response to neighbouring pillar recovery will be assessed.

### 3.1 Calculation of Initial Vertical Pillar Loads

The determination of the vertical stress acting on a pillar before and after adjacent pillar recovery is important for practical pillar design purposes. Given a specific panel geometry and a required safety factor, a knowledge of the vertical pillar load is conducive to the determination of pillar layouts and the optimisation of extraction.

Practical methods in estimation of vertical pillar loads have been a focus of research for many years. The tributary area method can be used to estimate the average pillar load

for a reasonably uniform pattern of pillars by assuming that each pillar bears a proportionate share of the total overburden load (Brady and Brown 2013). After mining exploitation, the vertical load  $\sigma_v$  on any remnant pillar is related to the initial overburden loading  $\rho g H$  and the near field extraction ratio  $e$ . But, this method does not account for interactions between adjacent pillars and between pillars and surrounding strata, possibly leading to a significant overestimation of vertical pillar loads (Roberts et al. 2002). Numerical modelling can be a tool to assess the stability of irregular pillars with local variations of the extraction ratio. On the basis of numerical results using a finite difference code, a quadratic fitting function of the relative extraction ratio was applied to estimate the average vertical pillar load (Hauquin et al. 2016). However, since the quadratic function is derived by simulating a variety of random panel layouts, it may not be applicable in analysing a specific pillar geometry. Poulsen (2010) developed a PAT-based method to calculate the average vertical stress acting on pillars of irregular geometries. Considering that pillars interact with adjacent pillars and surrounding strata within a lateral zone of influence, extraction ratios averaged over several pillars rather than the local extraction ratio for a single pillar are used in calculation. In this work, the PAT-based method was used to estimate initial vertical pillar loads and transferred loads after pillar recovery.

The load transfer distance (LTD) first introduced in the work of Abel (1988) represents the maximum distance that load can be transferred. Based on in situ measurements of 55 pillars within sedimentary deposits, the fitting quadratic function between the pillar depth  $H$  and the LTD is written as:

$$LTD = -1 \times 10^{-4} H^2 + 0.2701H \tag{1}$$

In the PAT-based method, the zone of influence (ZI) can be considered to be a circular area centred at the pillar with radius  $r$ , as illustrated in Fig. 2. Both  $r$  and ZI are associated with the LTD, and can be computed, respectively, by (Poulsen 2010):

$$r = 2LTD + w_e / 2 \tag{2}$$

$$ZI = \pi(2LTD + w_e / 2)^2 \tag{3}$$

where  $w_e$  is the effective width for non-square pillars, which is 4 times the ratio of pillar area to pillar circumference.

The vertical pillar load  $\sigma_v$  can be written as (Poulsen and Shen 2013):

$$\sigma_v = \frac{\rho g H}{1 - e} \tag{4}$$

where  $e$  is the extraction ratio in the ZI of the pillar, and is given by:

$$e = \frac{EA}{ZI} \tag{5}$$

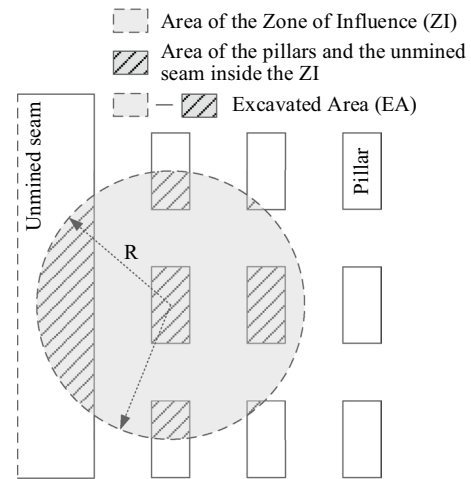


Fig. 2 Pillar geometry and the zone of influence used in the PAT-based method

where EA denotes the excavated area in the ZI, as illustrated in Fig. 2.

### 3.2 Calculation of Transferred Vertical Pillar Loads

After pillar recovery, the load previously carried by the removed pillar will be redistributed and act on neighbouring pillars or surrounding rock. For any pillar that remains unbroken, Eq. (4) can be used to estimate the vertical pillar stresses  $\sigma_v^0$  and  $\sigma_v^1$  before and after adjacent pillar recovery. If the removed pillar locates within the ZI of any pillar, the vertical load on that pillar would increase with the increase in its EA after pillar recovery. The increment in the vertical pillar load, termed as the transferred load, can be given by:

$$\Delta\sigma_s = \sigma_v^1 - \sigma_v^0 \tag{6}$$

For any pillar to support the transferred load,  $\Delta\sigma_s$  depends on the percentage of the area of the removed pillar to that of the ZI. However, the transferred load acts on adjacent pillars in a dynamic manner, and can thus be much larger in practical mining activities. In this regard, it is pertinent to compute the maximum induced vertical load and evaluate the pillar stability in a dynamics viewpoint, which will be described in Sects. 3.3 and 3.4 respectively.

### 3.3 Calculation of the Induced Dynamic Stress

Figure 3 illustrates the dynamic response of a pre-stressed pillar subjected to a suddenly applied load. The pillar is initially under compressional stress  $\sigma_v^0$ . When a transferred load is applied, the stress equilibrium is disturbed, and the pillar compression undergoes an acceleration stage until the vertical load reaches  $\sigma_v^1$ . At that moment, the vertical pillar stress

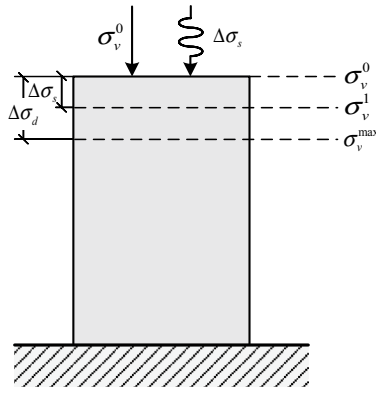


**Fig. 3** Dynamic response of a pre-stressed pillar subjected to a suddenly applied loading

is equal to the external load, indicating that it would be the equilibrium position for the pillar. Then, the speed of pillar compression declines until reaching the maximum compression position. The pillar would oscillate around and finally converge to the equilibrium position.

The induced disturbance to a pillar can be characterised by the dynamic amplification coefficient  $R$ , defined as the ratio of the dynamic increased vertical pillar load to the final transferred load. The maximum dynamic amplification coefficient  $R_{max}$  is achieved at the maximum compression position. The maximum vertical pillar load  $\sigma_v^{max}$  can be expressed in terms of  $R_{max}$ :

$$\sigma_v^{max} = \Delta\sigma_d + \sigma_v^0 = R_{max} \times \Delta\sigma_s + \sigma_v^0 \tag{7}$$

When a pillar is extracted using the blasting method, the support to the goaf roof is released in a very short time, and the overburden load is transferred to adjacent pillars. It is assumed that the load transfer duration is  $t_0$ . For any single neighbouring pillar, the time-dependent transferred load is considered to act as a single ramp loading followed by constant loading, as illustrated in Fig. 4. The loading history can be mathematically expressed as:

$$\sigma(t) = \begin{cases} \Delta\sigma_s \frac{t}{t_0} & t < t_0 \\ \Delta\sigma_s & t \geq t_0 \end{cases} \tag{8}$$

The pillar response to dynamic loads can be analysed by means of structural dynamics. Consider a dynamic impulse  $\sigma(\tau)$  acting on a static linearly elastic undamped system over time interval  $d\tau$  at time  $\tau$ , the resultant pillar response to the impulse at time  $t$  is:

$$y(t) = \frac{\sigma(\tau)d\tau}{m\omega} \sin \frac{2\pi}{T}(t - \tau), t \geq \tau \tag{9}$$

in which  $m$  and  $T$  are the mass and natural vibration period of the pillar, respectively. The mass and natural vibration period can be correlated by the elastic stiffness  $K$  of the pillar:

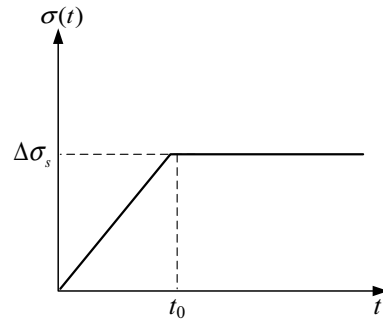


**Fig. 4** Loading history of a transferred pillar load

$$T = 2\pi \sqrt{m/K} \tag{10}$$

Equation (9) is approximate for finite impulse duration, and it becomes accurate when the duration approaches zero. The entire loading history  $\sigma(t)$  can be considered to consist of a succession of such short impulses, each giving rise to its own differential response. For the linearly elastic system, the total response can be obtained by integrating all differential responses over the loading time, which is known as the Duhamel integral equation (Clough and Penzien 2003):

$$y(t) = \int_0^t \frac{\sigma(\tau)}{m\omega} \sin \frac{2\pi}{T}(t - \tau) d\tau = \frac{T}{2\pi \times m} \int_0^t \sigma(\tau) \sin \frac{2\pi}{T}(t - \tau) d\tau, t \geq \tau \tag{11}$$

The pillar deformation in response to the time-dependent loading can be obtained by combining Eqs. (8, 10) and (11):

$$y(t) = \begin{cases} \frac{y_s}{t_0} \left( t - \frac{T}{2\pi} \sin \frac{2\pi}{T} t \right) & t < t_0 \\ y_s \left[ 1 - \frac{T}{\pi t_0} \cos \frac{2\pi}{T} \left( t - \frac{t_0}{2} \right) \sin \frac{\pi t_0}{T} \right] & t \geq t_0 \end{cases} \tag{12}$$

where  $y_s$  is the pillar deformation increment given by  $y_s = \Delta\sigma_s / K$ . For the linearly elastic pillar, the deformation is proportional to the induced vertical stress, which can be written as:

$$\frac{y(t)_{max}}{y_s} = \frac{\Delta\sigma_d}{\Delta\sigma_s} = R_{max} \tag{13}$$

Substituting Eqs. (12) to (13) gives the maximum dynamic amplification coefficient  $R_{max}$  in Eq. (7):

$$R_{max} = \max R(t) = \max \left[ \begin{array}{l} \frac{1}{t_0} \left( t - \frac{T}{2\pi} \sin \frac{2\pi}{T} t \right) t < t_0 \\ 1 - \frac{T}{\pi t_0} \cos \frac{2\pi}{T} \left( t - \frac{t_0}{2} \right) \sin \frac{\pi t_0}{T} t \geq t_0 \end{array} \right] \tag{14}$$



It can be observed from Eq. (14) that, given the natural vibration period  $T$ ,  $R_{\max}$  depends on the pillar recovery time  $t_0$ . To investigate the impact of pillar recovery time on dynamic response of adjacent pillars, the time-varying dynamic amplification coefficients for  $t_0 = 0, 0.01T, 0.5T, 1.0T$  and  $2.0T$  respectively is presented in Fig. 5.  $t_0 = 0$  means instantaneous pillar recovery, which yields an  $R_{\max}$  as much as 2. It can be seen that when  $t_0$  is shorter than  $0.01T$ ,  $R_{\max}$  approximates to that in the case of  $t_0 = 0$ . When the extraction time is longer than  $T$ ,  $R_{\max}$  becomes 1, suggesting no evidence of dynamic effect. When  $t_0$  ranges from  $0.01T$  to  $T$ ,  $R_{\max}$  falls in the range between 1 and 2.

Based on in situ microseismic measurements, the natural vibration period of rock masses is generally in a magnitude of  $10^{-1}$  s (Pan et al. 2007). Using the blasting method, the fragmentation of rock masses accompanied with the release of in situ stress takes places in several to ten milliseconds ( $10^{-3}$  to  $10^{-2}$  s) (Lu et al. 2012). Therefore, the induced dynamic amplification coefficient for a neighbouring pillar can exceed 1.5 or even approach 2.

### 3.4 Dynamic Instability Criterion for Pillar Workings

The conventional criteria for material failure can be classified into three types: stress/strain failure criteria, energy type failure criteria, and damage failure criteria (Li 2001). These criteria are usually applicable to stable or controlled failure phenomena, in which processes the failure takes place gradually and can be restrained by regulating the stress states.

However, in certain circumstances, uncontrolled failure phenomena such as rockbursts, pillar collapses and roof fall occur suddenly even without prior deterioration of the rock mass. These instances can be generalised as the problem of instability (Salamon 1970), and the failure criteria may be different. Salamon (1970) applied the complete stress–strain curve of uniaxial rock tests to the explanation of the pillar collapse phenomena, and suggested that pillars will be stable

if the sum of the stiffness matrix of mining workings and the slope matrix of the force–displacement curve of pillars is positive definite. In this respect, the stability conditions of pillars are dependent on their mechanical and deformation characteristics.

It is common that these phenomena involve both critical stress states of mine structures and external dynamic excitation. So, the external disturbance should be taken into account in evaluating the instability of mine structures. Petukhov and Linkov (1979) formulated a stability criterion based on the understanding of post-failure characteristics, which considers that instability occurs when the increment of external energy input exceeds the intrinsic energy increment. Zubelewicz and Mroz (1983) generalised the instability condition as the monotonic increase of the kinetic energy of the system under external excitations. This criterion was further examined by modelling two dynamic rock rupture phenomena induced by instantaneous excavation of pillars and a plane wave incidence to an excavation face, respectively. Li et al. (2005) and Zuo et al. (2005) used a catastrophic model to characterise the failure process of rock subjected to coupled static and dynamic loads, and found that the unstable failure is associated with both the magnitude and frequency of dynamic loads.

In this study, the rock mass is considered to become unstable when the released energy exceeds the energy consumed in the failure process (Dou et al. 2015). The criterion can be given by:

$$\frac{dU}{dt} = \frac{dU_s}{dt} + \frac{dU_d}{dt} > \frac{dU_f}{dt} \quad (15)$$

where  $U$  is the total released energy in the extraction,  $U_s$  is the strain energy stored in the rock mass to be extracted,  $U_d$  is the external energy from the dynamic disturbance, and  $U_f$  is the energy needed to be consumed in fracturing the rock mass. This criterion is applicable for rock masses under both two- and three-dimensional stress states.

For pillar workings under uniaxial compressive stress state, the total released energy is:

$$U = \frac{(\sigma_s + \sigma_d)^2}{2E} \quad (16)$$

where  $E$  is the elastic modulus of the pillar, and  $\sigma_s$  and  $\sigma_d$  are static and dynamic pillar loads, respectively.

Similarly,  $U_f$  can be computed using the critical stress  $\sigma_{\text{cri}}$ , i.e., the pillar load under the critical equilibrium state:

$$U_f = \frac{\sigma_{\text{cri}}^2}{2E} \quad (17)$$

Substituting Eqs. (16, 17) to (15), the criterion becomes:

$$\sigma_s + \sigma_d \geq \sigma_{\text{cri}} \quad (18)$$

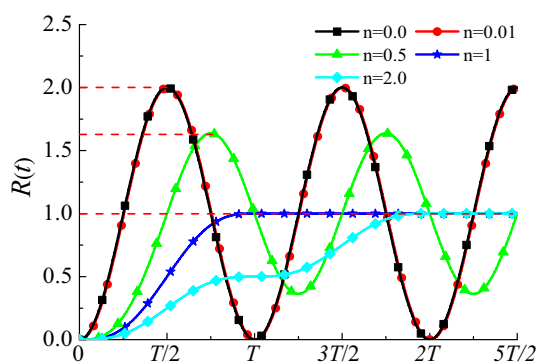


Fig. 5 Dynamic amplification coefficients of a pillar for different extraction time ( $n = t_0/T$ )

Combining Eqs. (7) and (18), the criterion in this study can be simplified to:

$$\sigma_v^{\max} \geq \sigma_{\text{cri}} \tag{19}$$

### 4 Numerical Simulation of Pillar Recovery Induced Disturbance

The theoretical formulation introduced in Sect. 3 indicated the significant impact of pillar recovery induced disturbance on the stability of neighbouring pillar workings. However, it assumed the disturbance to be a plane wave loading on a pre-stressed pillar, without considering the wave propagation from the removed pillar to remnant pillar workings. In addition, damping was not accounted for in the theoretical formulation.

In this section, the whole process including unloading wave emanation from pillar recovery, wave propagation in rock masses, and loading on remnant pillar workings, was numerically modelled. To limit this investigation to a controllable scope, a two-dimensional mining layout with five pillars of regular geometries were assumed. The discrete element method (DEM) based code PFC2D, was employed so as to explicitly model the dynamic rock failure.

#### 4.1 Model Setup and Calibration of Particle Parameters

PFC2D uses bonded contacts to model rock behaviour, and macroscopic properties of rock masses are determined by calibrated modelling properties of particles and contacts (Itasca 2008). The parallel-bond model is suitable to model brittle rock materials in that the parallel-bond establishes an elastic interaction between particles, transmitting both force and moment. This model features two sets of parameters, one set to control macroscopic deformation behaviour and the other to account for macroscopic strength characteristics.

Calibration of the numerical model is needed to obtain appropriate modelling properties of particles and contacts corresponding to macroscopic properties by matching numerical modelling results with experimental ones (Potyondy and Cundall 2004).

In this work, a hard rock pillar measuring 5 m × 5 m in Kaiyang Phosphate Mine were used in a numerical uniaxial

compression test for calibrating macroscopic rock behaviour against the empirical one. According to engineering geological survey reports and laboratory rock mechanical tests (Yao et al. 2012), the empirical compressive strength of the pillar is approximately 56 MPa and the elastic module is about 10 GPa. The obtained calibrated modelling parameters of particles and contacts are presented in Table 1.

A stratum model with dimensions of 101 m × 35 m (width × height) was constructed to represent a hard rock mining goaf area in Kaiyang Phosphate Mine (Fig. 6a). The explosive repulsion method (Itasca 2008) was adopted to generate the compacted assembly with a linear contact model. Particles with less than three contacts were deleted using a floater-elimination scheme embedded via a FISH function, and then the linear contact model was replaced by the parallel-bond model.

To model the successive collapses of pillar workings induced by sudden pillar recovery, the constructed model should have a pillar to be removed, a pillar immediately

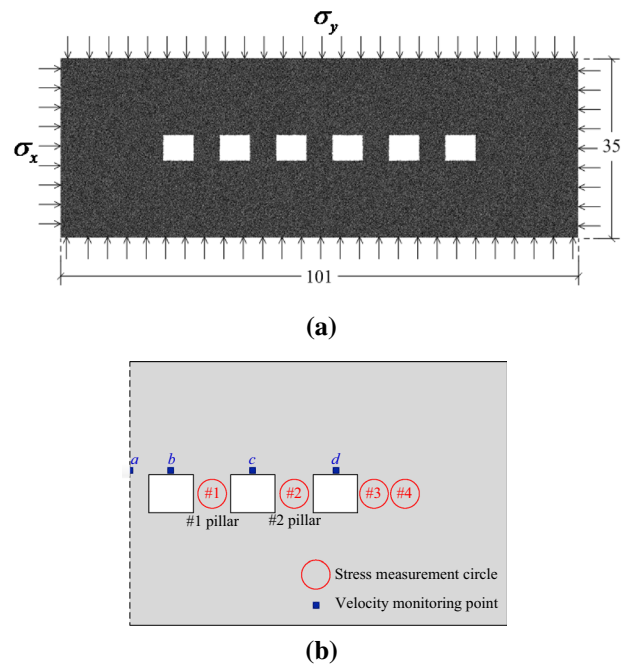


Fig. 6 Model geometry and measurement setup: a goaf model geometry with five pillars, and b setup of stress measurement circles and velocity monitoring points in the right half of the model

Table 1 Calibrated parameters of particles and contacts parameters used in the PFC2D model

Particle basic parameters		Parallel-bond parameters	
Particle density $\rho$ (kg/m <sup>3</sup> )	3220	Mean normal strength $\bar{\sigma}$ (MPa)	77
Minimum radii $r_{\min}$ (m)	$4.5 \times 10^{-2}$	Mean shear strength $\bar{\tau}$ (MPa)	38.5
Ball size ratio $r_{\max}/r_{\min}$	1.5	Elasticity modulus $\bar{E}_c$ (GPa)	10
Particle contact module $E_c$ (GPa)	10	Stiffness ratio $\bar{k}_n/\bar{k}_s$	4
Stiffness ratio $k_n/k_s$	4		

adjacent and another not immediately adjacent to the pillar to be removed. Unlike in the frame of continuum-based numerical modelling, the geomechanical response of rock masses (stress, displacement and failure behaviour) of a symmetrical model, obtained from the discrete element-based numerical approach, is not necessarily symmetrical, so it would be necessary to model the behaviour of adjacent pillars on each side of the pillar to be removed. In view of the computational efficiency achieved, it was found that a model consisting of five pillars, one central pillar to be removed and two adjacent pillars on each side, was adequate to demonstrate the dynamic process induced by sudden pillar recovery without a loss of generality. To this end, six  $6 \text{ m} \times 5 \text{ m}$  (width  $\times$  height) rooms with a spacing of 5 m were extracted, leaving five pillars to support the overburden load. The mining area was underlain and overlain by two hard rock layers of 15 m in height, respectively. Considering that stress states at a distance of 3 times of excavation sizes away from the mined-out area are unaffected by the excavation, the model is sufficiently large to minimise far-field boundary effects.

On the basis of two in situ measurements in the mine, the vertical stress and the maximum horizontal principal stress at 400 m depth are  $\sigma_v = 15 \text{ MPa}$  and  $\sigma_{H_{\max}} = 14 \text{ MPa}$ , respectively (Li et al. 2010; Yao et al. 2012). To represent the most vulnerable conditions of pillar workings, the vertical and the maximum horizontal principal stress ( $\sigma_v$  and  $\sigma_{H_{\max}}$ ) were used as vertical and horizontal normal boundary stresses ( $\sigma_y$  and  $\sigma_x$ ), whilst no shear stress was applied on model boundaries. The application of boundary stresses will be described in the Sect. 4.2.

To monitor geomechanical response to pillar recovery, a total of four stress measurement circles were set up on remnant pillar workings and surrounding rock, and four velocity monitoring points on the room roof, as shown in Fig. 6b. In view of the axial symmetry of the model and the central pillar to be extracted, measurement circles and points were only arranged on the right half of the model. The pillar closest to the central pillar on the right side is called #1 pillar, and the second closest is called #2 pillar. The initial average vertical pillar load in the model was 33 MPa, yielding a safety factor of 1.70. The natural vibration period of pillars in the model was around 60 ms as measured from free vibration of pillars subjected to instantaneous dynamic excitation.

## 4.2 Modelling Procedure

Static and dynamic analyses of pillar recovery were carried out, respectively, depending on whether the dynamic process was considered. As the first step to investigate the stress concentration in remnant pillars in the vicinity of the pillar recovery region, static analysis of the goaf model is reasonable. The modelling procedure for the static analysis consists of the

following steps: (1) the central pillar was extracted via the DELETE command. (2) A servo-control loading algorithm implemented via a FISH function was invoked to apply in situ stresses to each boundary until the model equilibrated.

For comparison, the stress distribution on pillars and surrounding rock was also evaluated under in situ stresses in the goaf model without pillar recovery.

For the dynamic analysis, the modelling sequences as elaborated for the static analysis were reversed, which means that in situ stresses were first applied to model boundaries, followed by the central pillar extraction. Then, the model was run until the goaf model became stable or broken. To account for the influence of pillar recovery time on neighbouring pillar workings and surrounding strata, the model was run repetitively for pillar recovery time 0, 10, 30, 50 and 100 ms, respectively. The scenario with pillar recovery time 0 is equivalent to the instantaneous pillar recovery.

While instantaneous pillar recovery was realised by removing all particles comprising the pillar via the DELETE command, dynamic pillar recovery in a certain duration was realised by means of the excavation relaxation method (Cai 2008). To be specific, particles representing the central pillar were first removed, and layers of particles on the newly formed roof and floor were identified to apply a set of forces equivalent to the internal forces of the deleted particles. The unloading of pillar stress can be controlled in such a manner that these forces were reduced in accordance with a specific path. For the sake of comparison to the theoretical formulation, a linear unloading path was adopted in this simulation. A flowchart of the modelling procedure for both quasi-static and dynamic pillar recovery is shown in Fig. 7.

According to the manual of PFC2D (Itasca 2008), the damping coefficient  $\alpha$  is given by:

$$\alpha = \pi D \quad (20)$$

where  $D$  is the fraction of critical damping. When the dynamic analysis was conducted, low numerical damping was specified in the model to simulate realistic levels of attenuation in rock mass. In this study, the local damping coefficient is set to 5% of critical damping. In addition, a 1 m thick particle layer with high viscous damping ( $\alpha = 0.5$ ) was assigned on each boundary, so as to prevent seismic waves from being reflected by model boundaries. The timestep for dynamic analysis was automatically determined based on the particle mass and the sum of stiffnesses acting on the particle.



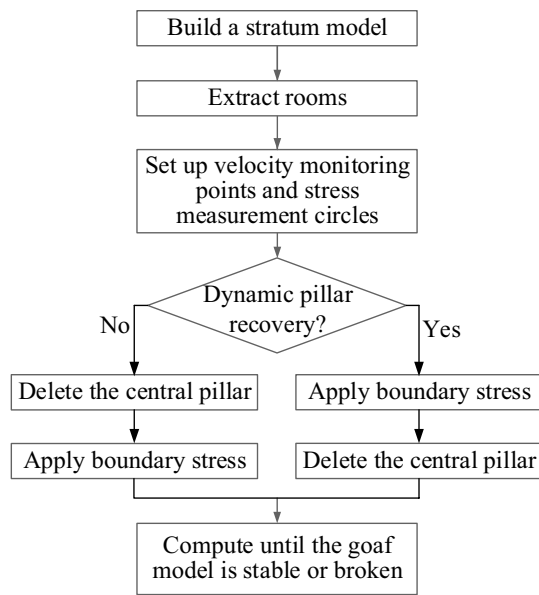


Fig. 7 Flowchart for numerical simulation of pillar recovery

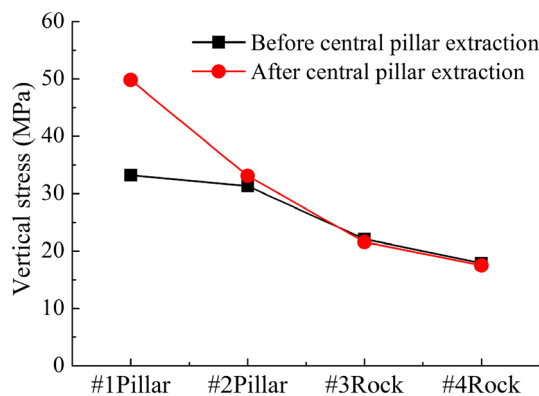


Fig. 8 Vertical loads for neighbouring pillars before and after central pillar recovery in static analysis

## 5 Modelling Results

### 5.1 Static Analysis of the Stability of Pillar Workings

Figure 8 shows the vertical stress states for pillars and surrounding rock before and after the central pillar recovery in static analysis. It can be observed that pillars closer to the removed pillar tend to carry more overburden during the load redistribution process. After the central pillar recovery, there are stress increases of 6.6 and 1.8 MPa in #1 and #2 pillars, respectively, but barely no stress increases in rock masses within #3 and #4 measurement circles, which means that only the stress concentration in pillars is aggravated. The safety factor for the most stressed #1 pillar is reduced

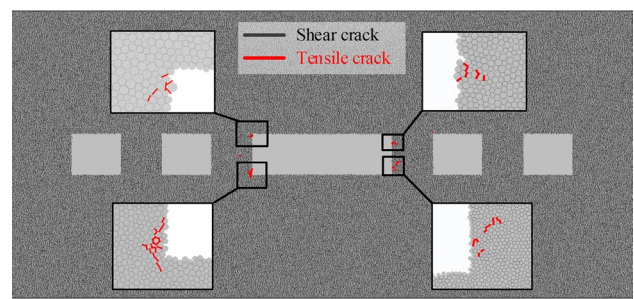


Fig. 9 Crack distribution on neighbouring pillars after central pillar recovery in static analysis

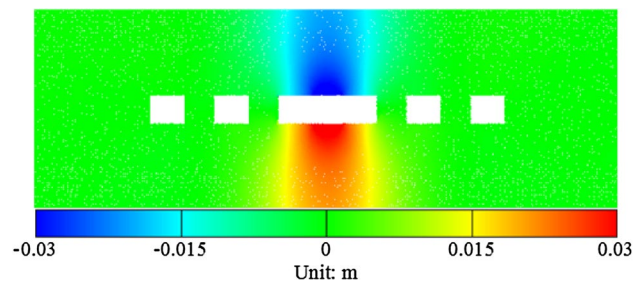


Fig. 10 Vertical displacement contour after central pillar recovery in static analysis

to 1.12, and the vertical load on the #1 pillar can be as much as 2.8 times of that on rock masses within the #4 measurement circle.

As illustrated in Fig. 9, the bearing capability of all remnant pillars remains unaffected, with only a few tensile cracks forming on the nearest two pillars on sides close to the removed pillar. Figure 10 presents the vertical displacement contour after pillar recovery. As no pillar collapses after the central pillar recovery, the displacement contour is symmetrical, and the induced floor heave and roof subsidence primarily fall between the two pillars most adjacent to the central one. The maximum displacement is around 30 mm, which occurs on the newly formed roof and floor during the pillar recovery process. This suggests that the influenced regions of pillar recovery are quite limited in the static analysis.

### 5.2 Dynamic Analysis of the Stability of Pillar Workings

#### 5.2.1 Instantaneous Pillar Recovery

Characterised by the shortest extraction time, the instantaneous pillar recovery process can cause the most remarkable dynamic excitation and most severe destruction in surrounding rock strata. In this section, only dynamic behaviour of surrounding rock and pillars in response to instantaneous

pillar recovery is presented, and the influence of pillar recovery time will be shown in Sect. 5.2.2.

Figure 11 illustrates the propagation of stress wave arising from the central pillar. In the figure, all referred times are elapsed times after the central pillar is extracted. It can be seen that the stress wave front reaches the nearest two pillars in 5 ms, and reaches the other two in 10 ms. However, it is noted that the wave front is of low velocity, and that the nearest pillars would not achieve the maximum velocity until 10 ms. In addition, the maximum induced vibration velocity attenuates rapidly during propagation. For example, the maximum recorded velocity at 10 ms reduces to as less as one-fifth that at 1 ms.

The vertical vibrations recorded at different velocity monitoring points are presented in Fig. 12. Since the point *a* locates on the newly formed roof, the vibration at the point *a* initiates almost at the same time of the instantaneous pillar recovery and peaks at 4.29 m/s. From 0.9 ms after the pillar recovery, vibration arises at points *b*, *c* and *d* chronologically, with a time lag of around 5 ms. The maximum velocity recorded at these points are 1.85, 0.79 and 0.26 m/s, respectively, which also indicates the quick attenuation of stress wave with travelling distance.

Figure 13 presents the variation of vertical stresses acting on remnant pillars and surrounding stratum after the central pillar recovery. The stress on the #1 pillar increases from 33.2 MPa to the pillar strength 56 MPa at around 30 ms, and then gradually decreases to a residual value (less than 5 MPa), which means it cannot carry much overburden any more. Except for the dynamic pillar recovery induced disturbance, transferred vertical loads from the collapsed pillars are detrimental to the stability of remnant pillars. After the collapse of the #1 pillar, stress applied on the #2 pillar quickly increases to the pillar strength and crushes the pillar.

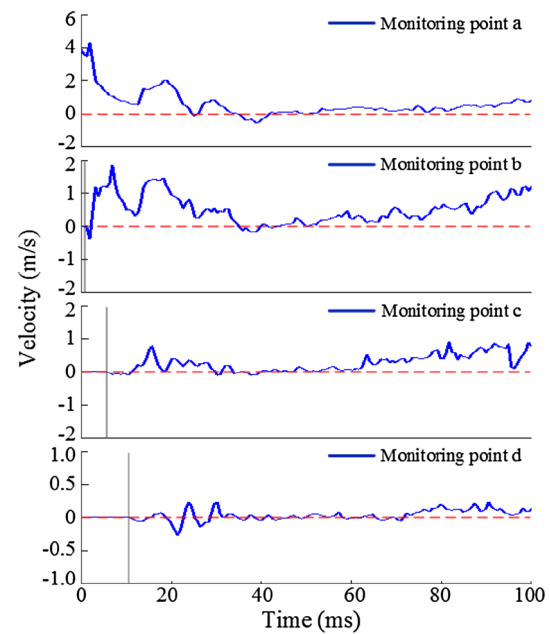


Fig. 12 Vertical velocity–time history of monitoring points

This is followed by marked increases in stresses on rock masses in #3 and #4 stress measurement circles, and the failure of rock masses in the #3 measurement circle. The final vertical stress on rock masses in the #4 measurement circle reaches about 80 MPa. In this way, the instantaneous extraction of a single pillar may trigger the domino instability characterised by a chain reaction of pillar collapses, leading to severe hazards over large underground stope areas. In addition, triggered pillar collapses can in turn induce disturbance in surrounding rock masses. For example, vibrations at monitoring points *b* and *c* begin to increase due to rock

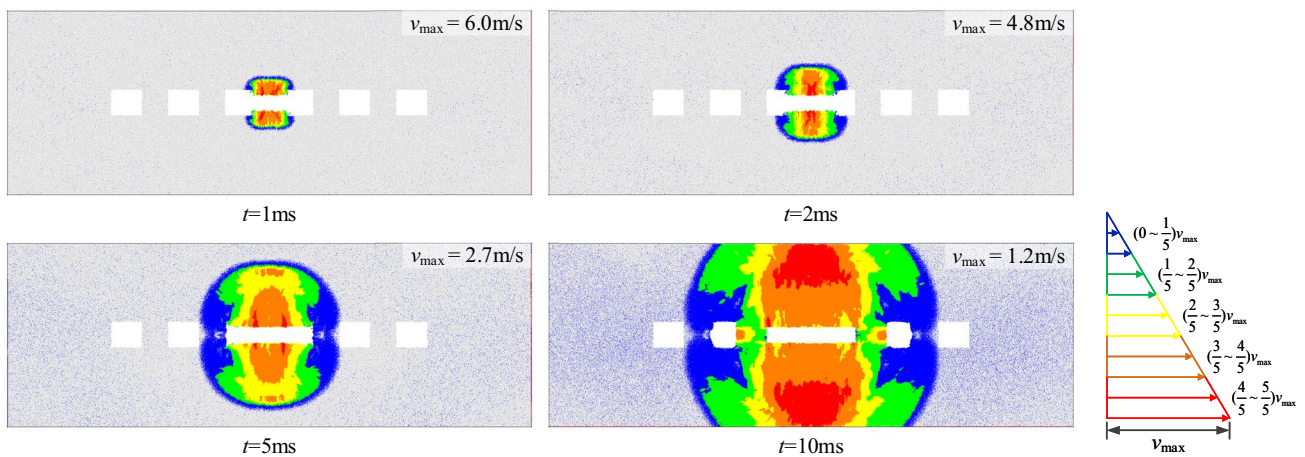
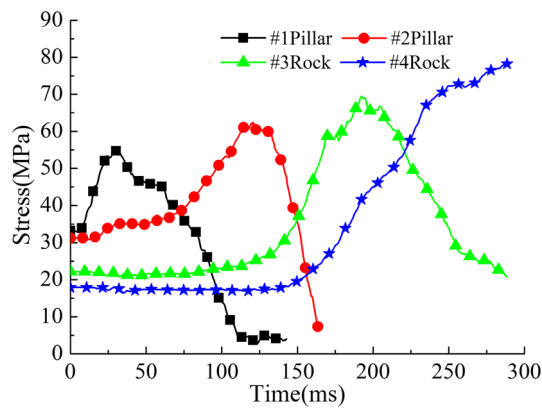


Fig. 11 Velocity contour after instantaneous pillar recovery



**Fig. 13** Vertical loads on pillars and surrounding rock over time after instantaneous pillar recovery

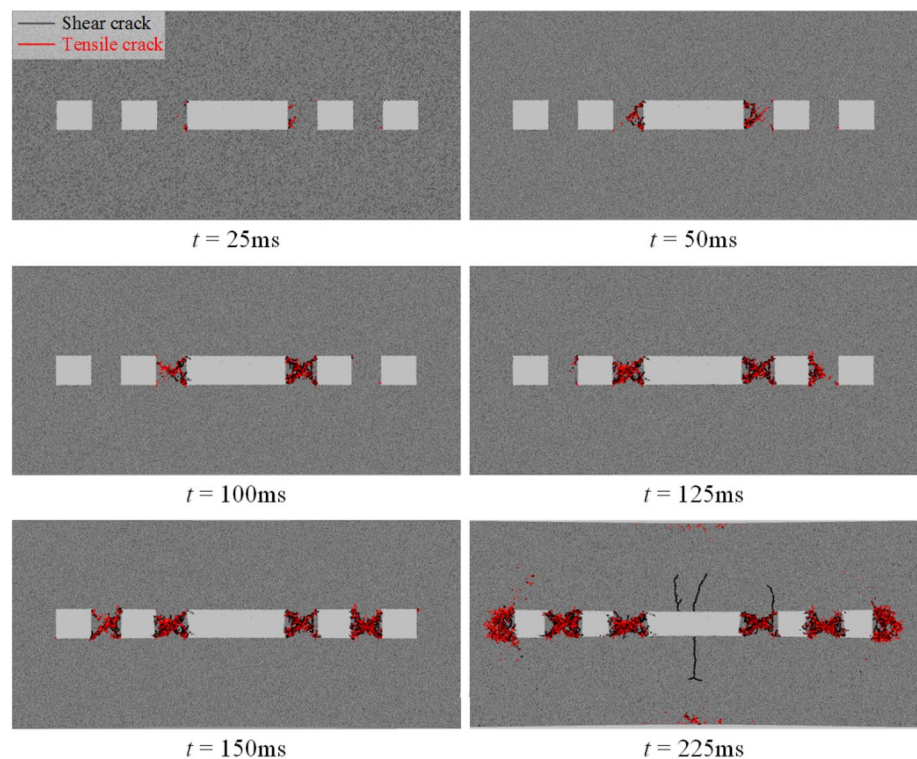
failure at around 60 ms, and the velocity at the monitoring point b can reach up to 1 m/s at 100 ms, as observed in Fig. 12.

Figure 14 illustrates the crack propagation over time after the central pillar is suddenly removed. Both tensile and shear cracks form in adjacent pillars subjected to the instantaneous pillar recovery. Induced pillar collapses take place in succession, from pillars nearest to the central pillar to farther ones. For all pillars under the dynamic disturbance, cracks first emerge at corners between pillars and roof or floor on sides close to the removed pillar, and then

grow gradually. When the pillar is approaching its supporting capacity, cracks propagate rapidly and finally coalesce into distinct X-type macroscopic failure. For example, only a few cracks occur in the two pillars closest to the central pillar at the beginning, and the crack number increases tremendously after 25 ms. After all pillars collapse, overburden previously carried by those pillars is transferred to surrounding rock and result in severe damage. In addition, macroscopic shear cracks initiate from both the newly formed roof and floor and propagate in the vertical direction at 225 ms, indicating the instability of the goaf model. It is noted in the figure that crack distribution does not remain symmetrical in shape. This is because granules of rock masses are represented by bonded circular disks, and the random particle packing geometry introduces intrinsic heterogeneity in crack initiation and propagation. New cracks tend to occur and grow in the vicinity of old ones where stress concentrates, and crack localisation is thus exacerbated.

The displacement contours at time steps corresponding to those in Fig. 14 are plotted in Fig. 15. Different from results of continuum-based software, the displacement contours extracted from PFC2D are not symmetrical. This is because a relatively large displacement is caused by the bond breakage between two rock granules, and localised crack concentration would result in asymmetrical displacement distribution. At 25 ms, the maximum displacement reaches 30 mm, and the zone of influence is limited

**Fig. 14** Crack distribution on pillars and surrounding rock after instantaneous pillar recovery





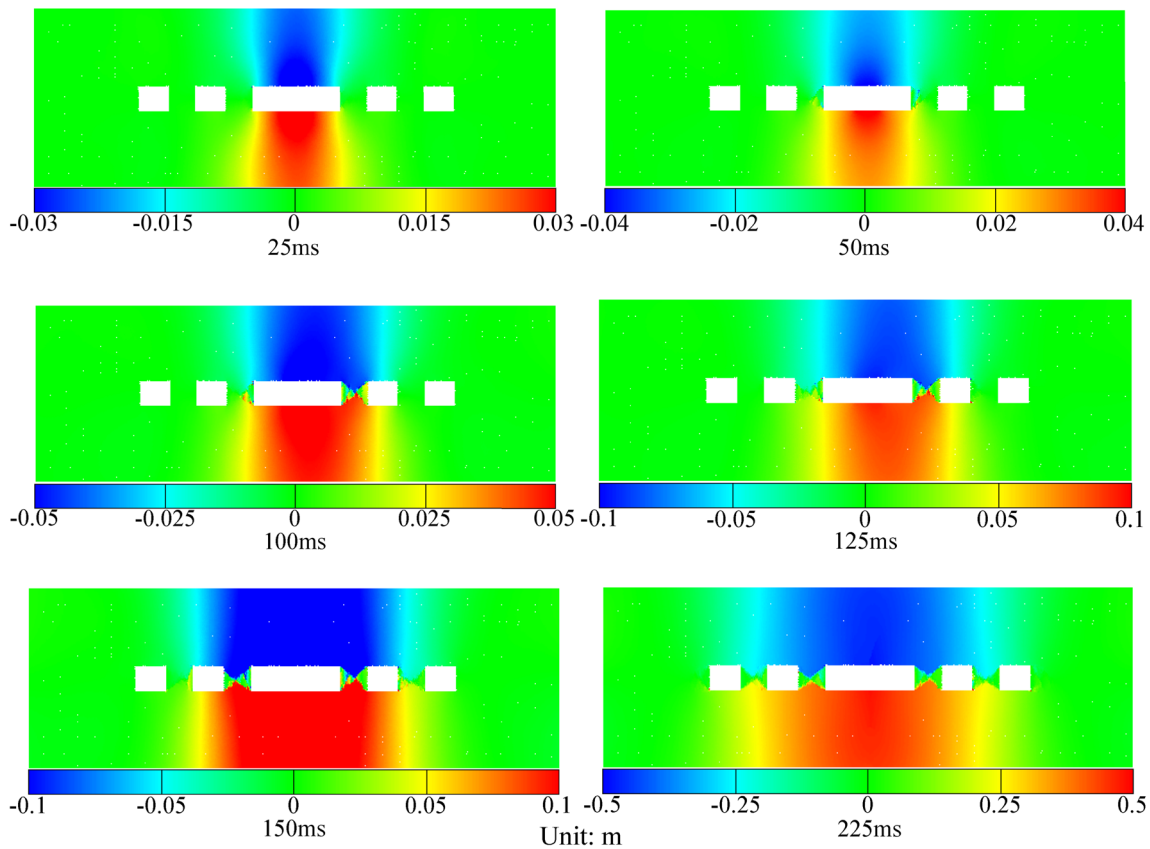


Fig. 15 Vertical displacement contours after instantaneous pillar recovery

between the two pillars nearest to the central one, which is quite similar to that in the static analysis. The zone of influence expands as pillars collapse progressively, finally spanning the whole pillar region. The largest displacement can reach up to 500 mm at 225 ms, more than 16 times that obtained from the static analysis.

### 5.2.2 Influence of Extraction Time on Dynamic Pillar Response

Figure 16 plots the dynamic mechanical state of the #1 pillar during the pillar recovery process for different extraction time. With a natural vibration period of around 60 ms, the extraction durations correspond to 0, 0.17 $T$ , 0.5 $T$ , 0.83 $T$  and 1.67 $T$ , respectively. Remarkable dynamic disturbance can be observed for scenarios with extraction time 0, 10 and 30 ms. In these three scenarios, the #1 pillar is crushed after the vertical load exceeds the pillar strength, and a residual stress far lower than the initial vertical stress is reached, indicating the loss of the bearing capacity. The dynamic pre-peak stress variation in the scenario with extraction time 10 ms is quite close to that of the instantaneous pillar recovery. For extraction durations 50 and 100 ms, the dynamic pillar response to the disturbance is almost negligible, and the pillar load

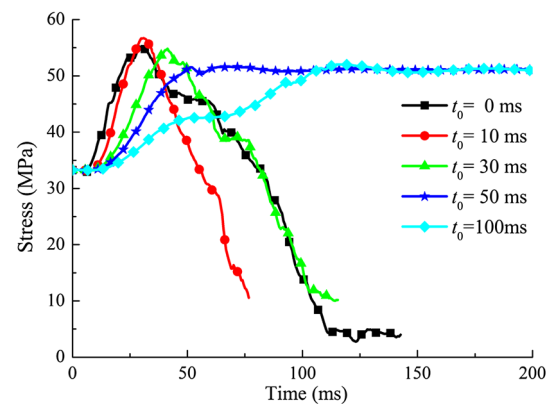
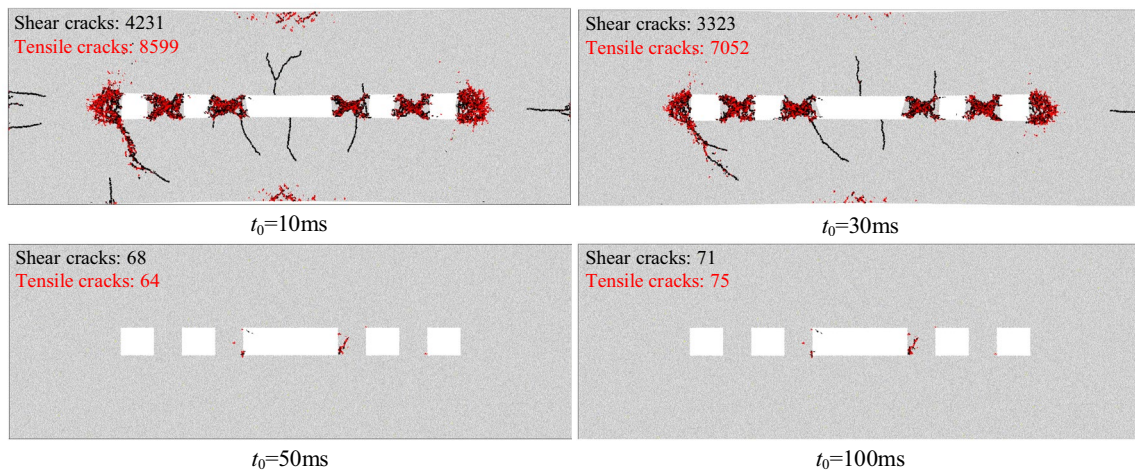


Fig. 16 Vertical load on the #1 pillar over time after dynamic pillar recovery

stabilises at about 50 MPa after pillar recovery. It is noted that stress variations in these two scenarios compare favourably with variations of  $R$  in Fig. 5.

Figure 17 presents the crack distribution at 225 ms for different recovery durations of the central pillar. For scenarios with extraction durations 10 and 30 ms, the disturbance caused by the central pillar recovery triggers relatively



**Fig. 17** Crack distribution on pillars and surrounding rock at 225 ms for different recovery durations of central pillar

violent pillar collapses and overall instability of the goaf model. Tensile cracks are more likely to be induced, and X-type macroscopic failure pattern could be observed in collapsed pillars, which is quite similar to the scenario of instantaneous pillar recovery. In contrast, no neighbouring pillars are crushed for scenarios with extraction durations 50 and 100 ms, and only a few cracks take place on incident sides of the dynamic disturbance. Results of stress variation and crack distribution show that the pillar recovery time is a significant factor influencing the induced dynamic behaviour of pillars.

## 6 Discussion

The present theoretical analysis verified that sudden loading on a pre-stressed pillar can generate remarkable dynamic excitation. The entire process of dynamic pillar recovery, wave propagation and loading on neighbouring pillars was then modelled, and results suggested that the dynamic pillar recovery induced disturbance has a significant influence on the stability of neighbouring pillars. While only small displacements occur in a limited region in the vicinity of the removed pillar in the static analysis, the domino instability of neighbouring pillar workings will take place in response to dynamic pillar recovery.

The influencing factors of the behaviour of neighbouring pillar workings can be classified into three categories: pillar strength, static stress levels, and dynamic stress levels. Static stress levels mainly depend on initial stress states and mining layouts (pillar width, pillar spacing and  $W/H$  ratios, etc) (Wang et al. 2016). Dynamic stress levels are associated with the pillar recovery process characterised by extraction duration, and seismic wave attenuation which is in turn related to pillar spacing and rock mass properties, etc. It is worth

noting that the impact of the distance from the removed pillar is twofold. In terms of static stress distribution, a short distance between residual pillars and the removed one is preferable for the sake of supporting overburden and increasing safety factors. On the other hand, strong dynamic disturbance can be caused in surrounding pillars by extraction of a pillar located in close vicinity. However, the seismic wave rapidly attenuates with travelling distance, and the induced dynamic effect could thus be minimal when residual pillar workings are far from the removed one, as per Figs. 11 and 12.

From theoretical and numerical analyses, it was recognised that if pillars are extracted in a quasi-static manner, no excitation would be induced in surrounding strata, and a neighbouring pillar remains stable as long as the sum of the initial load  $\sigma_v^0$  and final transferred load  $\Delta\sigma_s$  is less than the pillar strength (Fig. 18a, b). However, given the initial load and pillar strength, the failure state and stress state of a pillar in response to sudden pillar recovery depend on the incident dynamic excitation. Figure 18 illustrates time-varying vertical pillar loads after sudden extraction of a neighbouring pillar for two cases, in first of which the pillar collapses, but not in the latter one. Once the total pillar vertical load exceeds the critical stress (Eq. 19), the pillar is crushed, and the vertical stress drops to a residual stress far lower than the initial stress, suggesting that the load undertaken by this pillar is mostly added to the transferred load (Fig. 18a); otherwise the pillar oscillates at the natural frequency of rock masses, and the pillar vertical load eventually converges to the final stress state, same as that reached in the quasi-static extraction scenario (Fig. 18b).

It is noted that the time of pillar collapse caused by dynamic disturbance is not concurrent with that when the maximum pillar vibration velocity is reached. For example, the maximum vibration velocity of the #1 pillar is achieved



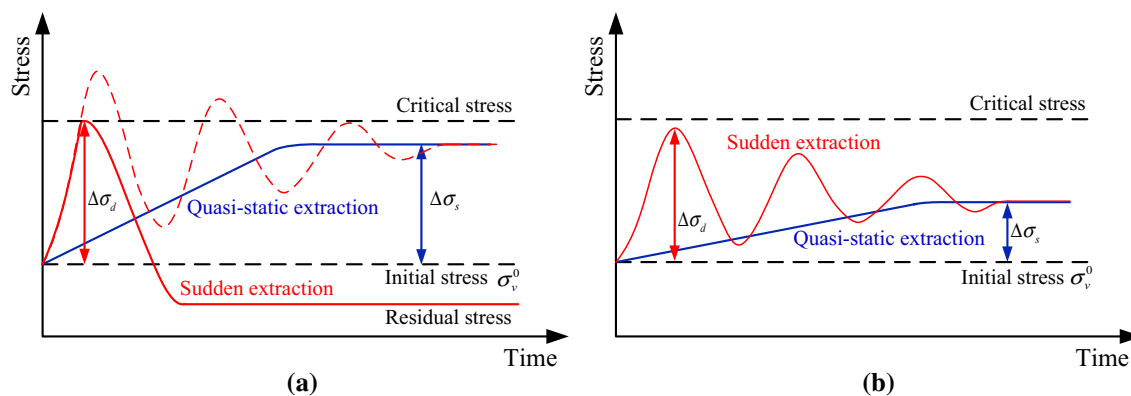


**Fig. 18** Schematic of rock failure criterion considering combined static and dynamic loads: **a** stress variation over time if failure occurs; and **b** stress variation over time if failure does not occur

at 10–15 ms (as estimated from Figs. 11, 12), and the pillar is crushed at around 30 ms (as shown in Fig. 13). This is because the maximum velocity is always achieved at the equilibrium position of the pillar (with deformation  $\Delta\sigma_s$  in Fig. 3), while the maximum stress is reached when the pillar is further compressed (with deformation greater than  $\Delta\sigma_s$  in Fig. 3). The failure state of pillars is evaluated based on the vertical pillar load rather than the pillar vibration velocity.

## 7 Conclusions

The stability of pillar workings is of significant importance in mining exploitation. In the present study, a mechanistic model was developed to evaluate the load acting on a pillar adjacent to a dynamically removed pillar on the basis of the pressure arch theory (PAT) based method and structural dynamics. In the model, pillars are assumed to be linearly elastic before failure occurs. For any pillar in the vicinity of the removed one, it is under combined effects of the initial static vertical load and the pillar recovery induced dynamic stress. The induced disturbance to a pillar can be characterised by the dynamic amplification coefficient  $R$ , the ratio of the increased vertical pillar load to the transferred load. The calculation results showed that  $R_{\max}$  is associated with the extraction time and the natural vibration period of rock mass. In practice pillar recovery using the blast method, the extraction time is one to two orders of magnitude lower than the natural vibration period of rock mass, and  $R_{\max}$  can exceed 1.5 or even approach 2.

The stability of neighbouring pillar workings subjected to dynamic extraction of the central pillar in a two-dimensional five-pillar system was then simulated in both static and dynamic modes using PFC2D. The influence of pillar recovery time on the stability of adjacent pillars was also investigated. The dynamic response of neighbouring pillar workings obtained in simulation was in good agreement

with those calculated using the mechanistic model, and both results indicated that the dynamic pillar disturbance can be reduced by increasing the pillar recovery time. In addition, it was found that pillars adjacent to the removed pillar remain stable in the static analysis, whilst the goaf model is unstable subjected to dynamic pillar recovery in the dynamic analysis. These results indicated that the maximum load carried by pillar workings would be largely underestimated if the dynamic effect resulting from pillar recovery is ignored in the design of pillar workings. Pillar workings designed to small safety factors can be considered as stable according to conventional methods, while in fact domino pillar instability can be triggered in the event of dynamic disturbance. For the sake of mining safety, it is recommended to account for the dynamic pillar recovery induced disturbance in the design of the pillar recovery method.

**Acknowledgements** This research is supported by financial grants from the National Basic Research Program of China (2015CB060200), the National Natural Science Foundation of China (No. 41772313) and the Hunan Natural Science Foundation (2015JJ4067). The authors are very grateful to the financial contribution and convey their appreciation of the organization for supporting this basic research.

## References

- Abel JF (1988) Soft rock pillars. *Int J Min Geol Eng* 6:215–248. <https://doi.org/10.1007/BF00880975>
- Brady B, Brown E (2013) *Rock mechanics: for underground mining*. Springer Science & Business Media, New York
- Cai M (2008) Influence of stress path on tunnel excavation response—numerical tool selection and modeling strategy. *Tunn Undergr Space Tech* 23:618–628. <https://doi.org/10.1016/j.tust.2007.11.005>
- Cao W, Li X, Tao M, Zhou Z (2016) Vibrations induced by high initial stress release during underground excavations. *Tunn Undergr Space Tech* 53:78–95. <https://doi.org/10.1016/j.tust.2016.01.017>

- Cao W, Shi J, Si G et al (2018) Numerical modelling of microseismicity associated with longwall coal mining. *Int J Coal Geol* 193:30–45. <https://doi.org/10.1016/j.coal.2018.04.010>
- Chao X, Zheng H, Hou X, Zhang X (2015) A stability study of goaf based on mechanical properties degradation of rock caused by rheological and disturbing loads. *Int J Min Sci Technol* 25:741–747. <https://doi.org/10.1016/J.IJMST.2015.07.007>
- Chen Y, Ma S, Yu Y (2017) Stability control of underground roadways subjected to stresses caused by extraction of a 10-m-thick coal seam: a Case Study. *Rock Mech Rock Eng* 50:2511–2520. <https://doi.org/10.1007/s00603-017-1217-z>
- Clough R, Penzien J (2003) Dynamics of structures. Computers & Structures, Inc., New York
- Dou L, He J, Cao A et al (2015) Rock burst prevention methods based on theory of dynamic and static combined load induced in coal mine. *J China Coal Soc* 40:1469–1476 (in Chinese)
- Hauquin T, Deck O, Gunzburger Y (2016) Average vertical stress on irregular elastic pillars estimated by a function of the relative extraction ratio. *Int J Rock Mech Min Sci* 83:122–134. <https://doi.org/10.1016/j.ijrmmms.2015.12.004>
- Itasca (2008) Particle flow code in 2 dimensions. Itasca Consult. Gr. Inc., Minneapolis
- Kaiser PK, Cai M (2012) Design of rock support system under rockburst condition. *J Rock Mech Geotech Eng* 4:215–227. <https://doi.org/10.3724/SP.J.1235.2012.00215>
- Kaiser P, McCreath D, Tannant D (1996) Canadian rockburst support handbook. Geomechanics Research Centre, Laurentian University, Sudbury, Ontario
- Li QM (2001) Strain energy density failure criterion. *Int J Solids Struct* 38:6997–7013. [https://doi.org/10.1016/S0020-7683\(01\)00005-1](https://doi.org/10.1016/S0020-7683(01)00005-1)
- Li X, Zuo Y, Ma C (2005) Failure criterion of strain energy density and catastrophe theory analysis of rock subjected to static-dynamic coupling loading. *Chin J Rock Mech Eng* 24:2814–2824 (in Chinese)
- Li W, Ma C, Li K et al (2010) Measurement and distribution of 3D geostress in Kaiyang phosphate mine in Guizhou. *Min Technol* 10(5):31–33
- Li X, Cao W, Zhou Z, Zou Y (2014) Influence of stress path on excavation unloading response. *Tunn Undergr Space Tech* 42:237–246. <https://doi.org/10.1016/j.tust.2014.03.002>
- Li X, Cao W, Tao M et al (2016) Influence of unloading disturbance on adjacent tunnels. *Int J Rock Mech Min Sci* 84:10–24. <https://doi.org/10.1016/j.ijrmmms.2016.01.014>
- Li X, Li C, Cao W, Tao M (2018) Dynamic stress concentration and energy evolution of deep-buried tunnels under blasting loads. *Int J Rock Mech Min Sci* 104:131–146. <https://doi.org/10.1016/j.ijrmmms.2018.02.018>
- Lu W, Yang J, Yan P et al (2012) Dynamic response of rock mass induced by the transient release of in-situ stress. *Int J Rock Mech Min Sci* 53:129–141. <https://doi.org/10.1016/j.ijrmmms.2012.05.001>
- Lunder P, Pakalnis R (1997) Determination of the strength of hard-rock mine pillars. *CIM Bull* 90:51–55
- Pan Y, Zhao Y, Guan F et al (2007) Study on rockburst monitoring and orientation system and its application. *Chin J Rock Mech Eng* 26:1002–1011 (in Chinese)
- Pao Y, Mow C (1973) Diffraction of elastic waves and dynamics stress concentrations. Rand Corporation, New York
- Petukhov IM, Linkov AM (1979) The theory of post-failure deformations and the problem of stability in rock mechanics. *Int J Rock Mech Min Sci* 16:57–76. [https://doi.org/10.1016/0148-9062\(79\)91444-X](https://doi.org/10.1016/0148-9062(79)91444-X)
- Potyondy DO, Cundall PA (2004) A bonded-particle model for rock. *Int J Rock Mech Min Sci* 41:1329–1364. <https://doi.org/10.1016/j.ijrmmms.2004.09.011>
- Poulsen BA (2010) Coal pillar load calculation by pressure arch theory and near field extraction ratio. *Int J Rock Mech Min Sci* 47:1158–1165. <https://doi.org/10.1016/j.ijrmmms.2010.06.011>
- Poulsen BA, Shen B (2013) Subsidence risk assessment of decommissioned bord-and-pillar collieries. *Int J Rock Mech Min Sci* 60:312–320. <https://doi.org/10.1016/j.ijrmmms.2013.01.014>
- Roberts DP, van der Merwe JN, Canbulat I et al (2002) Development of a method to estimate coal pillar loading. Safety in Mines Research Advisory Committee, COL 709, pp 1–90
- Salamon MDG (1970) Stability, instability and design of pillar workings. *Int J Rock Mech Min Sci* 7:613–631. [https://doi.org/10.1016/0148-9062\(70\)90022-7](https://doi.org/10.1016/0148-9062(70)90022-7)
- Singh AK, Singh R, Maiti J et al (2011a) Assessment of mining induced stress development over coal pillars during depillaring. *Int J Rock Mech Min Sci* 48:805–818. <https://doi.org/10.1016/j.ijrmmms.2011.04.004>
- Singh R, Singh AK, Maiti J et al (2011b) An observational approach for assessment of dynamic loading during underground coal pillar extraction. *Int J Rock Mech Min Sci* 48:794–804. <https://doi.org/10.1016/j.ijrmmms.2011.04.003>
- Suorinen FT, Kaiser PK, Mgumbwa JJ, Thibodeau D (2011) Mining of orebodies under shear loading Part 1—case histories. *Min Technol* 120:137–147. <https://doi.org/10.1179/1743286311Y.0000000012>
- Suorinen FT, Mgumbwa JJ, Kaiser PK, Thibodeau D (2014) Mining of orebodies under shear loading Part 2—failure modes and mechanisms. *Min Technol* 123:240–249. <https://doi.org/10.1179/1743286314Y.0000000072>
- Tao M, Li X, Li D (2013) Rock failure induced by dynamic unloading under 3D stress state. *Theor Appl Fract Mech* 65:47–54. <https://doi.org/10.1016/j.tafmec.2013.05.007>
- Wang H, Jiang Y, Zhao Y et al (2013) Numerical investigation of the dynamic mechanical state of a coal pillar during longwall mining panel extraction. *Rock Mech Rock Eng* 46:1211–1221. <https://doi.org/10.1007/s00603-012-0337-8>
- Wang SL, Hao SP, Chen Y et al (2016) Numerical investigation of coal pillar failure under simultaneous static and dynamic loading. *Int J Rock Mech Min Sci* 84:59–68. <https://doi.org/10.1016/j.ijrmmms.2016.01.017>
- Xiao X, Xiao P, Dai F et al (2017) Large deformation characteristics and reinforcement measures for a rock pillar in the Houziyan underground powerhouse. *Rock Mech Rock Eng*. <https://doi.org/10.1007/s00603-017-1329-5>
- Yang J, Lu W, Chen M et al (2013) Microseism induced by transient release of in situ stress during deep rock mass excavation by blasting. *Rock Mech Rock Eng* 46:859–875. <https://doi.org/10.1007/s00603-012-0308-0>
- Yao J, Ma C, Li X, Yang J (2012) Numerical simulation of optimum mining design for high stress hard-rock deposit based on inducing fracturing mechanism. *Trans Nonferrous Met Soc China* 22:2241–2247. [https://doi.org/10.1016/S1003-6326\(11\)61455-6](https://doi.org/10.1016/S1003-6326(11)61455-6)
- Zhang G, He F, Jia H, Lai Y (2017) Analysis of gateroad stability in relation to yield pillar size: a Case Study. *Rock Mech Rock Eng* 50:1263–1278. <https://doi.org/10.1007/s00603-016-1155-1>
- Zhao T, Guo W, Tan Y (2018) Case Studies of rock bursts under complicated geological conditions during multi-seam mining at a depth of 800 m. *Rock Mech Rock Eng*. <https://doi.org/10.1007/s00603-018-1411-7>
- Zhou Z, Cai X, Ma D et al (2018a) Effects of water content on fracture and mechanical behavior of sandstone with a low clay mineral content. *Eng Fract Mech*. <https://doi.org/10.1016/j.engfracmec.2018.02.028>
- Zhou Z, Chen L, Cai X et al (2018b) Experimental investigation of the progressive failure of multiple pillar–roof system. *Rock Mech Rock Eng*. <https://doi.org/10.1007/s00603-018-1441-1>

- Zubelewicz A, Mroz Z (1983) Numerical simulation of rock burst processes treated as problems of dynamic instability. *Rock Mech Rock Eng* 16:253–274. <https://doi.org/10.1007/BF01042360>
- Zuo Y, Li X, Ma C et al (2005) Catastrophic model and testing study on failure of static loading rock system under dynamic loading. *Chin J Rock Mech Eng* 24:741–746 (in Chinese)

**Publisher's Note** Springer Nature remains neutral with regard to jurisdictional claims in published maps and institutional affiliations.